Remote Sensing Applications: Society and Environment 36 (2024) 101351

Contents lists available at ScienceDirect

Remote Sensing Applications: Society and Environment

journal homepage: www.elsevier.com/locate/rsase

Remote detection of asbestos-cement roofs: Evaluating a QGIS plugin in a low- and middle-income country

Pauline Gluski [a], Juan Pablo Ramos-Bonilla [b, c], Jasmine R. Petriglieri [d, e], Francesco Turci [d, f], Margarita Giraldo [b], Maurizio Tommasini [g], Gabriele Poli [h], Benjamin Lysaniuk [i, *]

[a] IRD, UMR Prodig, 93222, Aubervilliers, France
[b] Department of Civil and Environmental Engineering, Universidad de Los Andes, Bogotá, 111711, Colombia
[c] Collegium Ramazzini, 40010, Bentivoglio, Bologna, Italy
[d] "G. Scansetti" Interdepartmental Centre for Studies on Asbestos and Other Toxic Particulates, University of Turin, Italy
[e] Department of Earth Sciences, University of Turin, Via Valperga Caluso 32, Turin, I-10125, Italy
[f] Department of Chemistry, University of Turin, Via Pietro Giuria 9, Turin, I-10125, Italy
[g] Prato Campus of University of Florence, Piazza Giovanni Ciardi 25, 59100, Prato (PO), Italy
[h] Institute of Applied Physics "Nello Carrara", Italian National Research Council (IFAC-CNR), Florence, Italy
[i] CNRS, UMR Prodig, 93222, Aubervilliers, France

ARTICLE INFO

Keywords:
ACM roof mapping
Remote sensing
Image classification
Sibaté
Colombia

ABSTRACT

Machine learning, a subset of artificial intelligence, has emerged as a powerful tool for generating new knowledge from observations. In the realm of geographic information systems (GIS), machine learning techniques have become essential for spatial analysis tasks. Satellite image classification methods offer valuable decision-making support, particularly in land-use planning and identifying asbestos cement roofs, which pose significant health risks. In Colombia, where asbestos has been used for decades, the detection and management of installed asbestos is critical. This study evaluates the effectiveness of the RoofClassify plugin, a machine learning-based GIS tool, in detecting asbestos cement roofs in Sibaté, Colombia. By employing high-resolution satellite imagery, the study assesses the plugin's accuracy and performance. Results indicate that RoofClassify demonstrates promising capabilities in detecting asbestos cement roofs, achieving an overall accuracy score of 69.73%. This shows potential for identifying areas with the presence of asbestos and informing decision-makers. However, false positives remain a challenge, necessitating further on-site verification. The study underscores the importance of cautious interpretation of classification results and the need for tailored approaches to address specific contextual factors. Overall, RoofClassify presents a valuable tool for identifying asbestos cement roofs, aiding in asbestos management strategies.

1. Introduction

Machine learning tools, a branch of artificial intelligence, are based on the ability of a given system to generate new knowledge from a set of observations (Parki, 2009). Deep learning, which is a subset of machine learning, employs models and algorithms that

* Corresponding author.
E-mail addresses: pauline.gluski@ird.fr (P. Gluski), jramos@uniandes.edu.co (J.P. Ramos-Bonilla), jasminerita.petriglieri@unito.it (J.R. Petriglieri), francesco.turci@unito.it (F. Turci), mm.giraldo337@uniandes.edu.co (M. Giraldo), maurizio.tommasini@gmail.com (M. Tommasini), g.poli@ifac.cnr.it (G. Poli), benjamin.lysaniuk@cnrs.fr (B. Lysaniuk).

https://doi.org/10.1016/j.rsase.2024.101351
Received 11 April 2024; Received in revised form 30 July 2024; Accepted 9 September 2024
Available online 10 September 2024

emulate the neural network architecture of the brain (Jakhar and Kaur, 2020). The applications of machine learning and deep learning are vast, as they autonomously extract knowledge from training data for descriptive, predictive, and prescriptive purposes (Btown, 2021). Significant advancements facilitated by machine learning and deep learning tools can be observed in various scientific fields over the past decades. In medical diagnostics, these tools have played a crucial role in identifying certain types of cancers (Kononenko, 2001) (Shebab et al., 2022). They have also found applications in finance, aiding in measuring financial risk and detecting fraudulent activities (Ozbayoglu et al., 2020). Additionally, machine learning and deep learning have contributed to image analysis and object detection tasks, such as automated image classification for characterizing land use and recognizing objects from remotely captured data (Maxwell et al., 2018) (Li et al., 2022). In the context of geographic information systems (GIS) spatial analysis, these tools have emerged as a key solution (Introduction to deep learning). Their ability to perform semantic segmentation and classify images has proven particularly valuable for solving GIS spatial analysis problems (Yuan et al., 2021).

Satellite image classification methods offer valuable decision-making support for land-use planning, including applications such as assessing the potential for solar panel installation (Mohajeri et al., 2018) (Gassar and Cha, 2021) and measuring the vulnerability of buildings to seismic risk (Borfecchia et al., 2010). Moreover, these methods enable the large-scale spatialization of building roofs based on their constituent materials, employing an object-oriented approach (Walter, 2004) (Trevisiol et al., 2022). One significant aspect is the identification of asbestos cement (AC) roofing sheets that pose a health risk. All asbestos fibers are carcinogenic to humans (Group 1) (IARC, 2012), and exposure to these fibers can lead to non-neoplastic diseases like asbestosis or pleural plaques, as well as certain cancers including larynx, ovaries, lungs, or mesothelioma (INSERM (collective expertise), 1997). Although the extent of asbestos fiber exposure depends primarily on the corrosion level of the asbestos-cement sheets (Dyczek, 2006), there remains a risk of exposure, substantiated by numerous studies (Kottek and Yuen, 2022) (Spurny, 1989) (Lee and Kim, 2021a) (Ervik et al., 2021). The identification of asbestos roofs can be conducted on a large scale either through on-site inspections, which require a substantial budget, trained personnel, and time, or through a remote approach utilizing satellite images or data acquired by airborne sensors. The utilization of hyperspectral imagery (Krówczyńska et al., 2020) (Frassy et al., 2014) (Fiumi et al., 2012), as well as more conventional multispectral satellite data (Hikuwai et al., 2023) (Gibril et al., 2017) (Osińska-Skotak and Ostrowski, 2015) (Taherzadeh and Shafri, 2013) (Abbasi et al., 2022) (Tommasini et al., 2019), has demonstrated an increasing precision in identifying asbestos cement roofs and mapping them on a broader scale: classification tools generally range from traditional machine learning approaches, such as the random forest classification algorithm, to artificial intelligence methods like convolutional neural networks. Hyperspectral satellite imaging and data acquisition through airborne sensors should, by virtue of improved image resolution, lead to more accurate classifications (Krówczyńska et al., 2020) (Frassy et al., 2014) (Fiumi et al., 2012) (Szabó et al., 2014) (Kaplan et al., 2023) (Valdelamar et al., 2024). However, implementing such studies requires significant funding, which compromises the chances of large-scale replication, especially in low- or middle-income countries. Our work has the modest ambition of assessing the performance of a method that is easily understandable and relies on readily available satellite data at a moderate cost.

It is estimated that cumulative world production of asbestos was 181 million tons between 1900 and 2003 (Virta, 2006). The peak demand was reached in 1977 when 25 countries were producing 4.8 million tons per year, and asbestos products were manufactured by approximately 85 countries (Virta, 2006). In 1980, asbestos-cement products, including corrugated asbestos-cement sheets, represented 66% of asbestos consumption, rising to 76% in South America (Virta, 2006). By 2003, asbestos-cement products accounted for 85% of total asbestos consumption worldwide (Virta, 2006). Colombia followed similar trends, although the lack of official government figures brings some uncertainty regarding quantities. Based on figures provided by the asbestos industry during debates on legislation aiming for a complete asbestos ban in Colombia, it was reported that by 2015, 300 million square meters of asbestos roofing had been installed in the country (Ascolfibras). In the same year, there was an estimated annual production of 230,000 tons of fibrocement, equivalent to slightly over 19 million square meters of roofing, which were installed in 350,000 households annually (Ascolfibras). Throughout the entire operational history of asbestos-cement factories in Colombia, which commenced operations in 1942, asbestos-cement roofing was installed in 5 million households, particularly low-income families, resulting in one out of every two Colombians living or having lived in homes with asbestos-cement roofing (Ascolfibras). A complete asbestos-ban was reached in Colombia in 2019, which came into effect on January 1st, 2021 (Law, 1968/19). However, the ban does not solve the negative legacy of installed asbestos products, which is a major public health challenge that the country is currently facing.

The deterioration of asbestos-cement roofing sheets exposed to environmental elements is a significant concern, as it leads to the release of toxic asbestos fibers into the air (Campopiano et al., 2009). This deterioration occurs due to various factors such as exposure to atmospheric agents, mechanical actions like vibrations or maintenance interventions, and chemical reactions induced by water, sun, ice, wind, and pollutants like sulfur dioxide and acid rain (Campopiano et al., 2009). These agents cause corrosion, dissolution of soluble salts, carbonation, and erosion of the cement structure, resulting in the liberation of asbestos fibers (Campopiano et al., 2009). Additionally, colonization by moss and lichen further contributes to the decay of the roofing sheets, ultimately leading to the formation of a surface layer rich in easily liberated asbestos fibers (Campopiano et al., 2009).

The identification and quantification of asbestos cement roofs are critical challenges in the management of asbestos installations spanning several decades. This challenge becomes even more pressing in countries like Colombia, where a law prohibiting asbestos came into effect on January 1, 2021, after more than 80 years of asbestos production and consumption (Congreso de Colombia, 2019) (Flórez Gutiérrez et al., 2023). In low- and middle-income countries, high-resolution satellite imagery presents a viable and accessible approach for identifying asbestos-cement roofs. Tommasini et al. (2019) have developed the RoofClassify plugin (https://plugins.qgis.org/plugins/RoofClassify/), an open-source geographic information system plugin that utilizes the random forest algorithm within an object-oriented framework to classify roofs. The plugin has demonstrated reliable performance in identifying asbestos cement roofs in the Prato region of Italy. In our study, we aim to assess the applicability of this plugin in the Colombian context, characterized by more irregular roof compositions (in terms of both geometry and materials) and less reliable input data.

To evaluate the capabilities of RoofClassify in the Colombian context, we propose applying the methodology developed by Tommasini et al. in the urban center of Sibaté, located in the department of Cundinamarca, Colombia. There are two primary reasons for selecting this site. Firstly, Sibaté is the focus of a comprehensive study aiming to characterize the entire asbestos exposome following the discovery of the first mesothelioma cluster in Colombia (Ramos-Bonilla et al., 2019) and the identification of friable asbestos in the municipality's subsoil (Lysaniuk et al., 2020). Therefore, conducting the evaluation in Sibaté aligns with the broader research effort focused on understanding asbestos-related risks in the region. Secondly, the topographical characteristics of the city, with its elevated points, facilitate direct roof identification. This aspect is of utmost importance both for establishing the training layers required for the analysis and for evaluating the performance of the RoofClassify plugin. This work evaluates the performance of the RoofClassify plugin in classifying roof materials in the urban area of Sibaté, Colombia, where roof heterogeneity and the lack of crucial input data pose significant challenges. Unlike the initial testing area, Sibaté lacks geolocated asbestos-cement roof data and has an imprecise cadastre, complicating the application of vector masks to satellite images. To address these constraints, original procedures were implemented, such as in-situ localization of training layers and the use of less precise vector masks. Beyond assessing classification accuracy, this study provides methodological insights for applying this approach in regions with similar characteristics to Sibaté.

2. Data and methods

For this project, a significant portion of the methodology was based on adapting the elements presented by Tommasini et al. (2019). However, to ensure compatibility and functionality with QGIS LTR during the period of 2022–2023, it was necessary to update the RoofClassify plugin. To accomplish this, we enlisted the services of Oslandia (https://oslandia.com/) to perform the following tasks.

1. Transitioning the code from Python 2 to Python 3.
2. Upgrading from PyQt 4 to PyQt 5.
3. Reevaluating the necessity of certain dependencies, such as PyShp.
4. Integrating the required dependencies, such as SciKit Learn, into the plugin delivery.

These updates were completed in advance of our study, and the revised plugin was subsequently reuploaded to the QGIS libraries. This approach aligns with the Open Source philosophy embraced by the original developers of RoofClassify, ensuring that the updated plugin is available for the wider community. The step-by-step procedure and functioning of RoofClassify are detailed in the study by Tommasini et al. (2019).

2.1. Study area and data collection

Sibaté is a city located in the department of Cundinamarca, approximately 25 km southwest of the center of Bogotá, the capital of Colombia (see Fig. 1). The municipality is home to an industrial zone that is directly connected to the southern part of Bogotá via the Southern Highway (*Autopista Sur*). Sibaté gained prominence as the site of Colombia's first asbestos-cement plant, established in 1942 to meet the domestic demand for asbestos-cement roofing sheets, as well as water supply and drainage pipes. Since the mid-2010s, there has been ongoing research into the environmental and human health negative impacts resulting from asbestos use in Sibaté (Ramos-Bonilla et al., 2019; Lysaniuk et al., 2020; Cely-García et al., 2020). In order to apply a detection and classification method for asbestos cement roofs in Sibaté, a high-resolution multispectral image from DigitalGlobe's WorldView3 (WV3) sensor was purchased. Ultimately, we acquired both a panchromatic image and an orthorectified multispectral image, with their characteristics detailed in Table 1. The analysis of both images resulted in the production of a pansharpened image, integrating the high spatial resolution of the panchromatic image with the spectral information from the multispectral image.

To limit the spatial coverage and reduce the number of pixels for the classification process, we employed a vector mask on the pansharpened image. The purpose was to exclude areas that do not correspond to roofs from the analysis. In this study, we evaluated two types of masks with different spatial scales. The first type of mask, which aligned with the original methodology, utilized the "buildings" layer sourced from the Colombian cadastral database. The second type of mask, with a coarser granularity, corresponded to the parcels that contain the buildings. To obtain the necessary vector data, we downloaded the relevant information from the Agustin Codazzi Geographic Institute (IGAC) website: https://geoportal.igac.gov.co/contenido/datos-abiertos-catastro. It is important to note that the department code for Cundinamarca, where Sibaté is situated, is 25. By employing these masks, we aimed to refine the classification process and focus specifically on the areas that encompass buildings and their respective parcels, facilitating more accurate identification of roofs in the analysis.

2.2. Classification via RoofClassify

In this study, we followed the classification procedures outlined by Tommasini et al. (2019), which rely on machine learning techniques using a set of training layers. For the specific case of Sibaté, we identified four main types of roofs: concrete, terracotta tiles, asbestos cement, and zinc sheets. To create the training layers, fieldwork was conducted by two researchers who georeferenced several buildings representing each roof type. In total, we identified 13 concrete-roofed buildings, 29 buildings with zinc sheets, 44 buildings with tile roofs, and 28 buildings with asbestos cement sheets. These buildings were then manually identified on satellite imagery and vectorized into polygons, each classified according to its corresponding roof type (see Fig. 2 - left). These polygons served as training layers. To generate a pansharpened image, we employed the Relative Component Substitution (RCS) algorithm from the Orfeo ToolBox, an image processing software library originally developed by the French Space Agency. This algorithm integrates with the QGIS interface (https://www.orfeo-toolbox.org/) and merges the multispectral and panchromatic image data, utilizing the higher resolu-

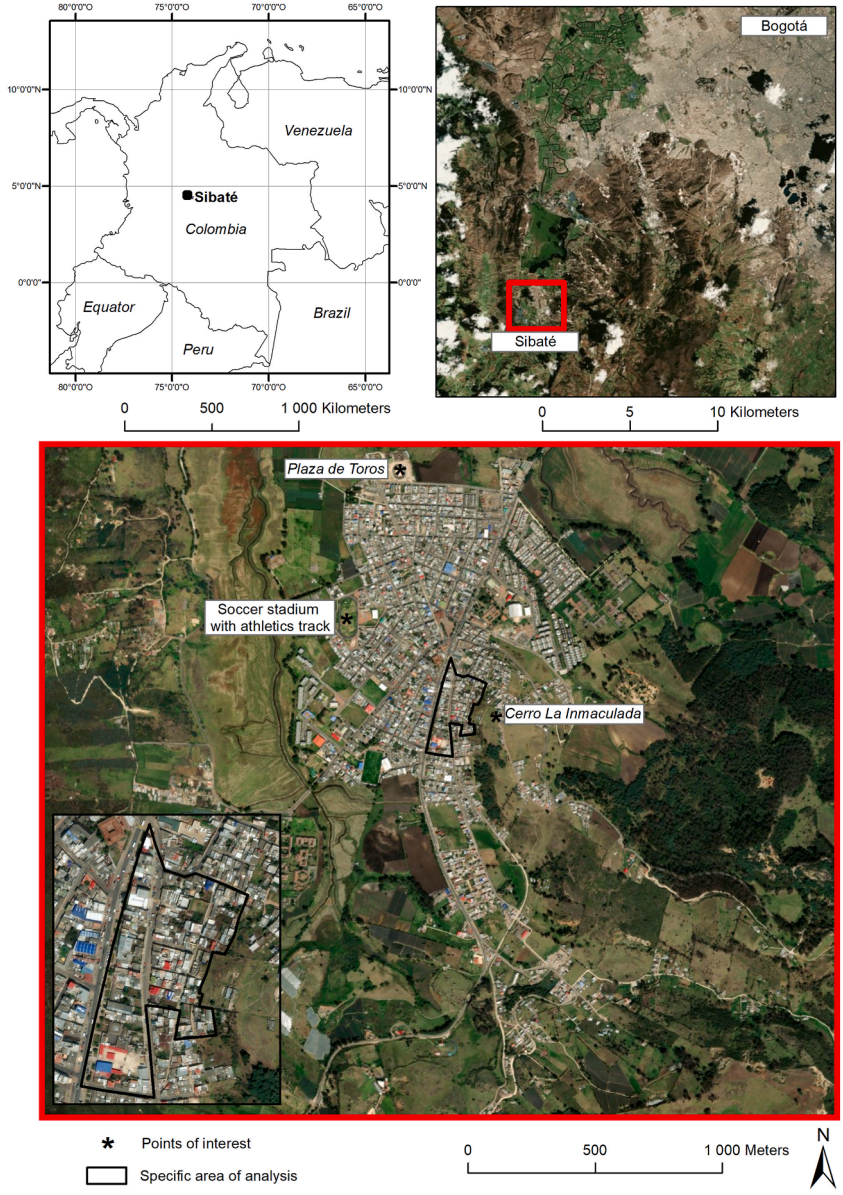

Fig. 1. Location of Sibaté (source: Digital Globe, 2016).

Table 1
Characteristics of the WV3 panchromatic (PAN) and multispectral satellite (MS) images used in this study.

Date and code of the scene	April 2, 2020 (1040010056605100)
Bands	8-Band Bundle
Resolution	30 cm (Pan)/1.2m (MS)
Kernel	MTF
Coordinate System	UTM
Datum	WGS84
Tiling	None
Bit Depth	16-Bit
File Format	GeoTiff
Product	OR2A
Media	FTP-Pull
DRA	Off

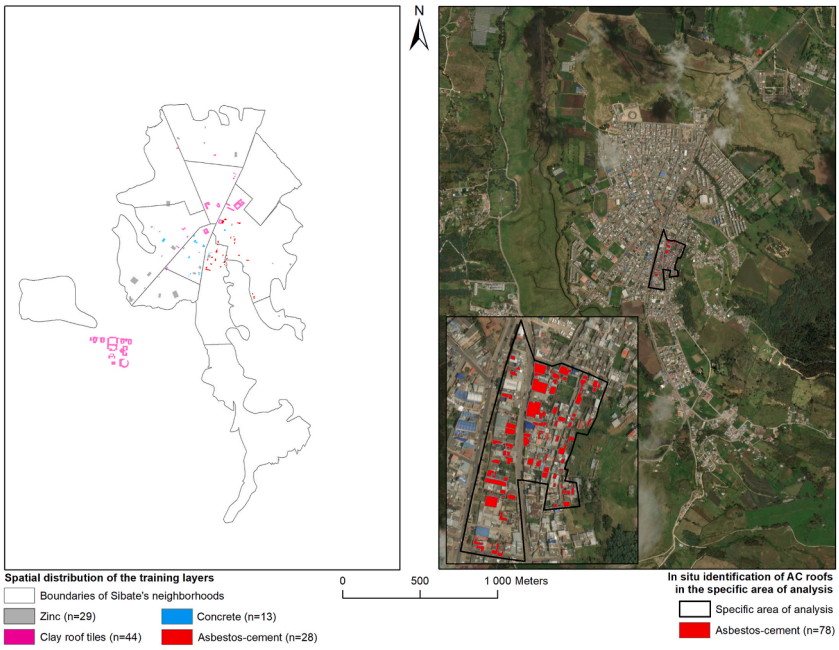

Fig. 2. Training layers and specific area of analysis.

tion of the panchromatic image. Following pansharpening, we used the ArcToolBox Cut Raster tool in ArcGIS (ESRI) to extract the relevant portion of the pansharpened raster. The vector masks employed in this step were derived from the "parcels" layer obtained from IGAC, as we encountered difficulties in rectifying the slight offset in the "building" layer. The goal of this step is to eliminate pixels that are not associated with the identified parcels, thus enhancing the accuracy of the subsequent classification. In our work, we did not implement the image partitioning step described by Tommasini et al. (2019) since the size of our image did not necessitate it. Consequently, we proceeded directly to the classification stage in RoofClassify. The user-friendly interface of the plugin facilitated the process, requiring the selection of the raster to be classified, the training layers, the raster associated with the training layers, and the destination folder for the output file. The interface also offers additional options, such as creating shape counts or percentages to provide information on the number or percentage of pixels per class within a given polygon. Upon completion of the classification, the plugin generates a raster image with pixels classified according to the training layers, allowing for the identification of different roof types across the study area. In summary, our classification method is based on the signals acquired by the spectral bands of the WorldView-3, in the visible (VIS) and near infrared regions (NIR). Therefore, the algorithm is based and trained on the matching between the fusion of signals in the VIS and NIR bands and the "in-situ" collected data in Sibaté. Additionally, to improve the results, the VIS and NIR measurements (acquired with different spatial resolutions) were scaled on the same geographical grids.

2.3. Classified image cleanup

Pixel-based classification using training layers can sometimes result in isolated pixels or "false positives" that are not associated with actual roofs. To address this issue, we employed the "sieve" utility, which is available in the "analysis" tools of the GDALTools extension in QGIS. This utility allowed us to remove raster surfaces below a user-defined threshold (s). The deleted surfaces were then replaced with the value of the largest adjacent surface. In our study, which adopted an exploratory approach, we conducted multiple trials using different pixel grouping threshold values: 5, 10, 15, 20, 25, 30, 35, and 40 aggregated pixels. This process helped to refine the cleaning of the classified raster by eliminating isolated pixels or small false positive areas. To further enhance the cleaning process, a second filter was applied. From the various sieved rasters obtained, we performed a raster-to-polygon conversion. This conversion referred to the polygons recognized automatically by the GIS based on the raster classification results. After converting to polygons only those areas suspected to be asbestos cement roofs that exceeded a certain surface area threshold value (a) were selected. Several surface area threshold values (5, 10, 15, and 20 m^2) were tested. This step ensures that only sufficiently large areas, likely to be actual roofs, are considered. In summary, isolated pixels were removed using the sieving tool, and then after converting the raster to polygons, asbestos-cement polygons below a certain area threshold were also removed. Thus, test several combinations from s5a5 to s40a40 were tested. By employing these filters and thresholds, we aimed to reduce the presence of noise and false positives in the classified results, focusing on asbestos cement roofs that are more likely to be accurate and meaningful.

2.4. Validation of "identified" roofs

To evaluate the agreement or discrepancies between the asbestos cement roofs detected by the RoofClassify plugin and the actual asbestos cement roofs on-site, we conducted another field trip. The purpose of this trip was to directly identify the asbestos cement roofs in a specific area. The selection of the observation area was based on two criteria: the presence of a high vantage point that pro-

vided a clear view of the roofs and the proximity (within 400 linear meters) to a densely built-up area for easier access. From *Cerro La Inmaculada*, located in the area (as shown in Fig. 1), three researchers equipped with binoculars conducted the *in-situ* identification of asbestos cement roofs. Each researcher independently identified the roofs, and their identifications were cross-checked by the other two researchers. To aid in the identification process, the researchers had a color printout of the satellite image of the area and marked the identified asbestos cement roofs on it. Subsequently, these marked roofs were vectorized using GIS software. The specific area we focused on resulted in the identification of 78 polygons corresponding to asbestos cement roofs (as depicted in Fig. 2 on the right side). These polygons represent the actual asbestos cement roofs observed on-site and serve as a reference for comparing the detection results obtained from the RoofClassify plugin.

2.5. Assessment of detection quality

The evaluation of the detection quality primarily involves comparing the "asbestos-cement roofs detected" layer generated by the RoofClassify plugin with the "asbestos-cement roofs observed" layer obtained from the on-site visual inspection. These two shapefile polygon layers were compared to determine the level of agreement.

By comparing these layers, we could measure the following.

1. Surfaces that match: These are the areas where the "asbestos-cement detected" layer and the "asbestos-cement observed" layer overlap or coincide, indicating successful detection by the RoofClassify plugin.
2. False positive surfaces: These are areas where the RoofClassify plugin detects asbestos-cement roofs, but they are not validated during the visual inspection. These represent instances where the plugin falsely identifies certain surfaces as asbestos-cement roofs.
3. False negative surfaces: These are areas where asbestos-cement roofs are present based on the visual inspection, but they are not detected by the RoofClassify plugin. These instances represent the roofs that are missed or undetected by the algorithm.

We performed these measurements within the specific analysis zone for each combination of filters applied to clean the image. This allows us to assess the detection quality and identify the optimal combination of filters that effectively reduce image noise (using the sieve operation and area threshold).

To analyze the accuracy and performance of the RoofClassify plugin in detecting asbestos-cement roofs and to determine the suitable filter combination, we conducted the following steps.

1. Intersect function: Using the intersect function in ArcGIS, we intersected the "fibrocement detected" layer (output of RoofClassify) with the polygon representing the zone of analysis. This operation resulted in a single layer representing the detected asbestos-cement roofs within the zone of analysis (denoted as A).
2. Intersect function: Next, we used the intersect function in ArcGIS between layer (A) and the "asbestos-cement installed" layer. This intersection generates matching surfaces, where the detected asbestos-cement roofs overlap with the actual installed asbestos-cement roofs (denoted as B). These areas represent the accurate detection by the plugin.
3. Erase function: To identify false positive surfaces, we used the erase function in ArcGIS between layer (A) and the "asbestos-cement installed" layer. This operation removes the areas where the detected asbestos-cement roofs coincide with the actual installed roofs, leaving behind the falsely detected areas (denoted as C). These surfaces represent instances where the plugin incorrectly identified non-asbestos-cement roofs as asbestos-cement.
4. Erase function: Similarly, we used the erase function in ArcGIS between the "asbestos-cement installed" layer and layer (A). This erase operation highlights the false negative surfaces (denoted as D), which correspond to the areas where the plugin failed to detect the actual asbestos-cement roofs present in the zone of analysis.

By performing these operations and analyzing the resulting layers (B, C, and D), we can evaluate the accuracy of the detection by comparing the detected roofs with the actual installed roofs. This assessment allows us to measure the true positive, false positive, and false negative rates and further refine the detection process by optimizing the filter combination.

In the final step of our analysis, we assessed the impact of the vector mask that corresponds to the parcels (i.e., “parcels” layer) and that was previously described, and a second vector mask composed of manually vectorized roofs was created, to substitute the imprecise “buildings” layer from the Colombian cadastral database. This latter mask was generated by accurately delineating the boundaries of asbestos-cement roofs through meticulous manual identification. Thus, we examined three scenarios. First, we evaluated the detection quality without a vector mask, considering the entire pansharpened image extent. This allowed us to measure the performance of the RoofClassify plugin in identifying asbestos-cement roofs without any spatial restrictions. Next, we used the "parcels" layer as the vector mask during the detection process. This layer represents the parcels or land plots in the study area. By limiting the analysis to the areas defined by the parcels, we aimed to focus the detection on the roofs within those boundaries, potentially improving the accuracy of the results. Finally, we used the manually vectorized roofs mask, to further enhance the detection quality by excluding non-roof areas and focusing solely on the specific roofs of interest. By comparing the results obtained under these three scenarios, we were able to quantify the impact of the vector masks on the detection quality within our test area.

2.6. Detection precision from an accuracy matrix

In addition, the classification performance at the pixel level across all types of roofs included in this work was measured. To do this, an "accuracy" post-processing tool from the SCP plugin (Congedo, 2021) developed for QGIS was applied. Thus, we determined the overall accuracy of the classification proposed by RoofClassify for all classes at Sibaté by comparing a set of in-situ identified roof data (zinc = 22 polygons, tiles = 21 polygons, concrete = 24 polygons, asbestos-cement = 78 polygons) with the pixels classified

by RoofClassify. Similarly, the matrix indicated true and false positives and highlighted metrics such as overall accuracy and the Kappa statistic.

2.7. Analysis of samples collected for validation purposes

In cases where the plugin yielded unexpected or counterintuitive results in terms of asbestos detection, field samples were collected from these locations for laboratory confirmation. If the detected surface was composed of solid concrete material, a sample of this material was collected. For detections on land surfaces, two samples of the material were collected for laboratory analysis — one from the surface and another from 4 cm below the surface.

For laboratory analysis, samples were preliminary dried at 300 °C for 3–5 h to remove organic matter (e.g., bitumen, roots, leaves) and sieved to obtain a fraction <100 μm. Scanning Electron Microscope (SEM) analyses were carried out with ZEISS EVO50 XVP equipped with an X-Stream OXFORD EDS. Secondary Electron and Backscattered Images were acquired at various magnifications (100x, 1000x, and 5000x) and accelerating voltages, commonly 5–10 kV. Microanalysis operating conditions were 10 kV, 100 pA, and 30 s counting time; relative wt% errors are $<1\%$ for major elements and $<5\%$ for minor components. Transmission Electron Microscopy (TEM) analyses were performed by a JEOL 1400 FLASH microscope, working at 100 kV, 15000x magnification. The microscope is equipped with STEM control and energy dispersive spectrometer (EDS Oxford X-Max 65T). Soil fractions were dispersed in ultrapure water (5 mg/1,5 ml) and sonicated for 30 s at 10 W. 10 μl of solution was deposited on mesh Cu grids with supporting lacey carbon films. 30 graticule areas were examined for each sample. Polarized Light Microscopy analyses coupled with Dispersion Staining method of observation (PLM-DS) were carried out with an Olympus BX51 microscope equipped with a phase contrast mask. Two aliquots were examined for each sample. Asbestos fibers identification was carried out with the oil immersion method, using the following Refractive Indices: for chrysotile and tremolite, RI 1.550 and RI 1.605 were used as advised by the UK - Health and Safety Executive (Health and Safety Executive, 2021). Non-chrysotile asbestiform serpentine was observed assigned with the intermediate RI 1.5680 (Petriglieri et al., 2020).

A workflow diagram summarizing all the steps of the methodology is presented in Fig. 3.

3. Results

3.1. Classification, image cleaning and detection quality

Upon completing the classification process with RoofClassify, we obtained an image that differentiated pixels into four categories representing our training layers: yellow for asbestos cement, blue for concrete, pink for clay tiles, and red for zinc. The resulting image (Fig. 4 - A) was generated using the "parcels" vector mask. A preliminary visual analysis of the image reveals several key observations. Firstly, there is a satisfactory spatial distribution of classified elements, indicating the presence of potential roofs throughout the study area. However, the image exhibits a notable level of noise and highlights the limitations of detection, particularly with numerous small-scale features down to the pixel level. Nonetheless, a significant number of distinct clusters, representing roofs, are clearly discernible. Additionally, a few larger elements stand out, primarily zinc roofs found on larger collective buildings such as gymnasiums, courtyards, and village halls. Remarkably, asbestos cement roofs appear to be present in all neighborhoods of Sibaté without exception, reflecting their widespread use. Nevertheless, some confusion arises in the classification. Certain access roads located to the north of the urban zone, which were not included in the vector mask, are erroneously identified as concrete sectors. Moreover, two specific areas present challenges as they are classified as potentially asbestos-contaminated despite not being roofs. These areas are the *Plaza de toros* (Bull ring) to the north and the athletics track to the west (Fig. 4 - A), both of which are public spaces.

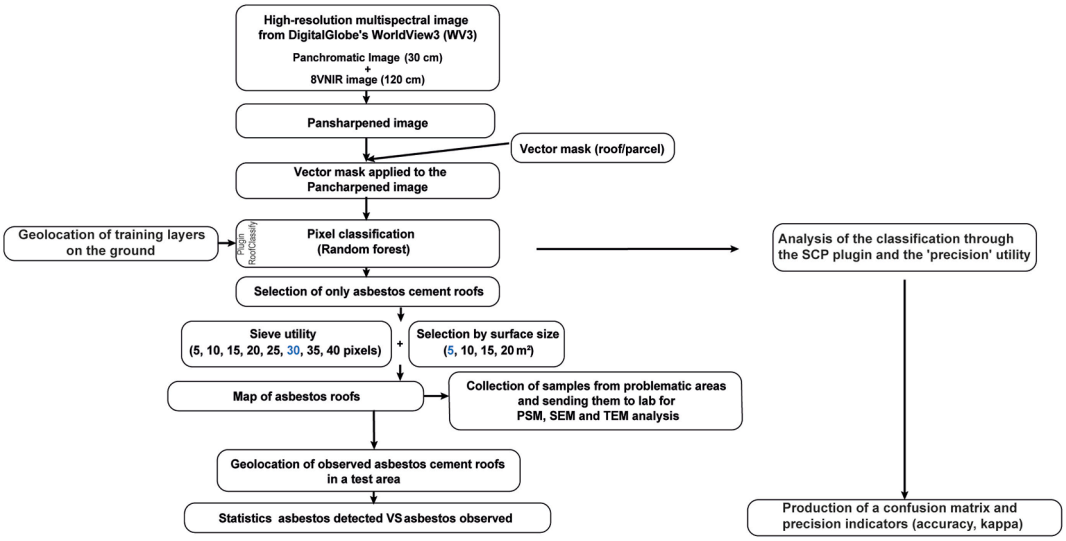

Fig. 3. Workflow diagram of the methodology.

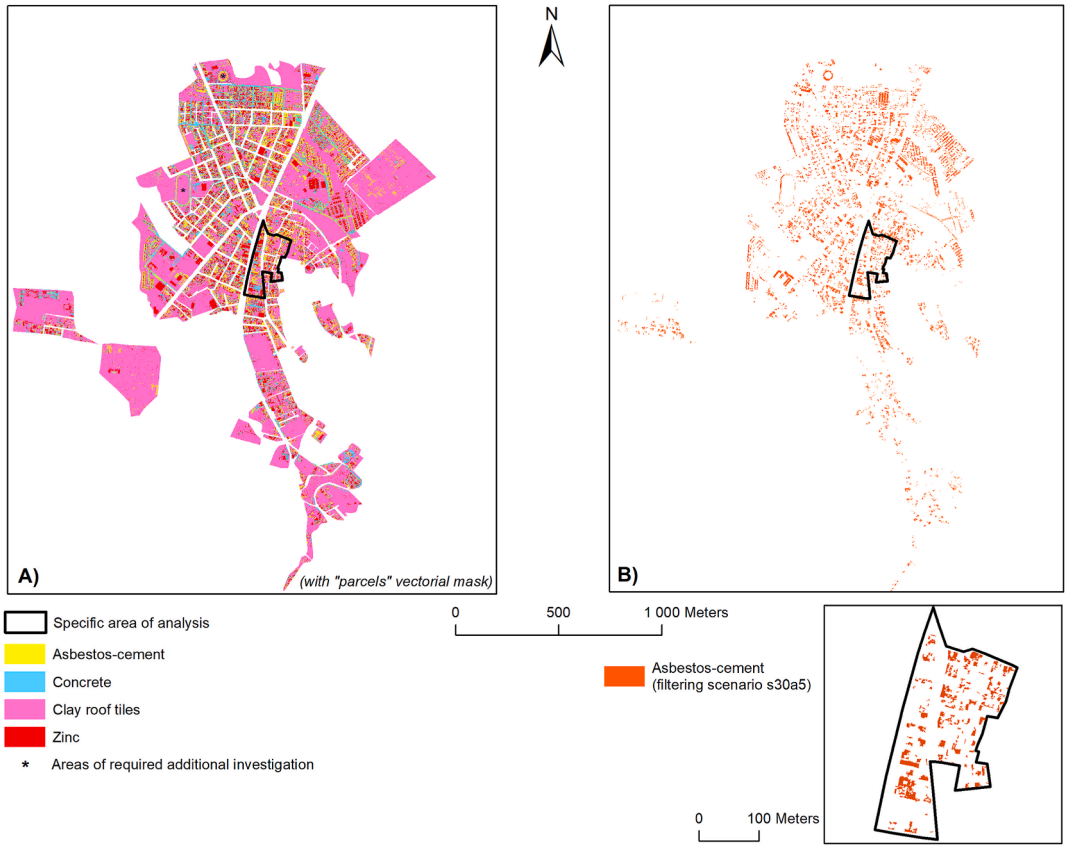

Fig. 4. RoofClassify image of Sibaté roofs.

Given the potential risks associated with activities taking place on the surfaces classified as potentially asbestos-contaminated, we deemed it necessary to collect samples from these areas. The samples were carefully collected and sent for analysis to a specialized laboratory at the University of Turin, which provide further insights into the presence of asbestos or other relevant substances. In addition, it is worth highlighting the large areas depicted as clay roofs when using the "parcel" vector mask, an unexpected result that is examined in detail in the discussion section.

The evaluation of the accuracy and performance of the RoofClassify plugin in detecting asbestos-cement roofs and the determination of the suitable filter combination showed that the best scenario for cleaning the classified image involved using a minimum aggregation threshold of 30 pixels of the same class combined with a minimum surface area of 5 m^2, referred to as "s30a5" (Table 2). This specific combination yielded the highest quality in terms of matching detected asbestos cement areas with installed areas. The analysis showed a perfect match of 53.34% between the installed and detected asbestos cement areas. However, it is important to note that there were still areas that were not detected by the classification, amounting to 46.66% of the installed areas, which are false negatives (Table 2). Despite this, the classification process, based on four training layers and a total of 114 polygons, successfully detected more than half of the installed asbestos-cement surfaces.

If the interpretation of the results is focused on the identification of polygons with at least the partial presence of asbestos-cement (*i.e.*, not in terms of surface), the detection results should be read differently. In this context, the RoofClassify plugin partially detected asbestos cement in 74 out of the 78 polygons that contained asbestos-cement roofs. However, it also produced 55 additional polygons erroneously classified as containing asbestos-cement (Table 3). It is important to note that the presence of false positives can have implications for the accuracy of the overall detection results. While the plugin successfully detects a considerable portion of the asbestos-cement surfaces in terms of surface area, the presence of false positives should be considered when analyzing the individual polygons and assessing the precise detection performance.

3.2. Measuring the importance of the vector mask in detection quality

The assessment of the impact of vector mask refinement on the quality of asbestos cement detection, showed upon visual inspection that the differences between these detection scenarios are not immediately apparent (Fig. 5).

The spatial distribution of detected asbestos-cement roofs shows minimal variation across different vector mask scenarios. Upon closer analysis of Fig. 5, it is possible to identify a few lines in the detection results without a vector mask (B), indicating potential misclassification of roads as asbestos cement. When comparing the detections using a "parcels" vector mask versus a "roofing" mask (Fig.

Table 2
Analysis of detection quality over a portion of our study area.

Sieving Scenarios	Areas of installed fiber-cement roofs (visual identification)	Areas of fiber-cement roofs detected by Roofclassify	Concordance - Areas of fiber-cement roofs detected by Roofclassify and validated by visual identification	False positive - Areas of fiber-cement roofs detected by Roofclassify but not validated by visual identification	False negative - Areas of installed fiber-cement roofs not detected by Roofclassify
s5a5	6386,91m^2	5273,4m^2	3327.46m^2 (52.1%)	1945.95m^2 (36.9%)	3059.55m^2 (47.9%)
s5a10	6386,91m^2	4993,86m^2	3256.60m^2 (50.99%)	1737.25m^2 (34.79%)	3130.46m^2 (49.01%)
s5a15	6386,91m^2	4757,16m^2	3180.70m^2 (49.8%)	1576.47m^2 (33.14%)	3206.31m^2 (50.2%)
s5a20	6386,91m^2	4528,02m^2	3108.55m^2 (48.67%)	1419.47m^2 (31.35%)	3278.45m^2 (51.33%)
s10a5	6386,91m^2	5349,33m^2	3366.09m^2 (52.7%)	1982.97m^2 (37.06%)	3020.85m^2 (47.3%)
s10a10	6386,91m^2	5084,28m^2	3293.84m^2 (51.57%)	1790.17m^2 (35.21%)	3093.01m^2 (48.43%)
s10a15	6386,91m^2	4820,85m^2	3217.93m^2 (50.38%)	1602.66m^2 (33.24%)	3168.86m^2 (49.62%)
s10a20	6386,91m^2	4626,27m^2	3144.56m^2 (49.23%)	1481.47m^2 (32.02%)	3242.27m^2 (50.76%)
s15a5	6386,91m^2	5367,4m^2	3387.46m^2 (53.03%)	1979.76m^2 (36.88%)	2999.45m^2 (46.96%)
s15a10	6386,91m^2	5118,64m^2	3321.60m^2 (52%)	1796.89m^2 (35.1%)	3065.31m^2 (47.99%)
s15a15	6386,91m^2	4870,41m^2	3259.91m^2 (51.04%)	1610.46m^2 (33.06%)	3126.96m^2 (48.96%)
s15a20	6386,91m^2	4641,64m^2	3170.74m^2 (49.64%)	**1470.76m^2 (31.68%)**	3216.12m^2 (50.35%)
s20a5	6386,91m^2	5412,55m^2	3394.73m^2 (53.15%)	2017.77m^2 (37.28%)	2992.23m^2 (46.85%)
s20a10	6386,91m^2	5145,52m^2	3328.87m^2 (52.12%)	1816.59m^2 (35.30%)	3058.11m^2 (47.88%)
s20a15	6386,91m^2	4896,21m^2	3267.18m^2 (51.15%)	1629.09m^2 (33.27%)	3119.74m^2 (48.85%)
s20a20	6386,91m^2	4685,71m^2	3178.01m^2 (49.76%)	1507.66m^2 (32.17%)	3208.9m^2 (50.24%)
s25a5	6386,91m^2	5397,68m^2	3404.44m^2 (53.3%)	1993.18m^2 (36.93%)	2982.47m^2 (46.7%)
s25a10	6386,91m^2	5149,01m^2	3330m^2 (52.14%)	1918.96m^2 (37.27%)	3056.83m^2 (47.86%)
s25a15	6386,91m^2	4854,53m^2	3276.61m^2 (51.3%)	1577.87m^2 (32.5%)	3110.28m^2 (48.7%)
s25a20	6386,91m^2	4680,47m^2	3187.43m^2 (49.9%)	1492.98m^2 (31.9%)	3199.45m^2 (50.09%)
s30a5	6386,91m^2	5382,77m^2	**3406.52m^2 (53.34%)**	1986.24m^2 (36.9%)	**2980.53m^3 (46.66%)**
s30a10	6386,91m^2	5150,85m^2	3339.63m^2 (52.29%)	1811.2m^2 (35.16%)	3047.3m^2 (47.71%)
s30a15	6386,91m^2	4867,8m^2	3286.25m^2 (51.45%)	1581.55m^2 (32.49%)	3100.74m^2 (48.55%)
s30a20	6386,91m^2	4708,86m^2	3212.19m^2 (50.29%)	1496.65m^2 (31.78%)	3174.80m^2 (49.71%)
s35a5	6386,91m^2	5399,03m^2	3405.79m^2 (53.32%)	1993.19m^2 (36.92%)	2981.25m^2 (46.68%)
s35a10	6386,91m^2	5154,95m^2	3338.91m^2 (52.28%)	1815.99m^2 (35.23%)	3048.01m^2 (47.72%)
s35a15	6386,91m^2	4882,61m^2	3285.52m^2 (51.44%)	1597.05m^2 (32.71%)	3101.47m^2 (48.56%)
s35a20	6386,91m^2	4723,67m^2	3211.47m^2 (50.28%)	1512.16m^2 (32.01%)	3175.53m^2 (49.72%)
s40a5	6386,91m^2	5387,29m^2	3397.26m^2 (53.19%)	1989.99m^2 (36.94%)	2989.85m^2 (46.81%)
s40a10	6386,91m^2	5133,40m^2	3330.38m^2 (52.14%)	1802.99m^2 (35.12%)	3056.61m^2 (47.86%)
s40a15	6386,91m^2	4882,3m^2	3278.94m^2 (51.34%)	1603.34m^2 (32.84%)	3108.07m^2 (48.66%)
s40a20	6386,91m^2	4723,36m^2	3204.88m^2 (50.18%)	1518.44m^2 (32.15%)	3182.14m^2 (49.82%)

Table 3
Detecting asbestos roofs.

Sieving scenario	Installed fiber-cement roofs (number of polygons)	Detected fiber-cement roofs (number of polygons)	Number of polygons representing installed fiber-cement roofs in which a detection was performed	Number of polygons representing detected asbestos cement roofs outside the polygons representing installed roofs
s30a5	78	129	74 (94,87%)	55 (42,63%)

5 C vs D), the differences are primarily observed in the polygon geometry and the number of polygons, rather than in the overall spatial distribution.

Therefore, in our study area the use of a vector mask and its spatial resolution has only a marginal influence on the quality of detection. As expected, a more precise vector mask leads to smaller areas of detected asbestos cement, resulting in a lower percentage of false-positive areas, which decreases to approximately 26% when using a "roof" vector mask (Table 4). However, the refinement of the vector mask does not seem to significantly impact the concordance between the detected and installed asbestos-cement areas. These findings suggest that while the spatial resolution and accuracy of the vector mask can affect the size and number of detected asbestos-cement polygons, they have limited impact on the overall quality of detection in terms of concordance. It should be noted that 'total area' does not exactly correspond to the sum of 'concordance' and 'false positives'. The slight differences observed are due to rounding and the conversion from 'raster to polygons', which affects the areas.

Across all three scenarios, the percentage of perfectly matching surfaces exceeds 50% (Table 4, Concordance), indicating a relatively good concordance between the detected and installed asbestos-cement areas. Interestingly, when using a fine vector mask (i.e., roofing), the main improvement is observed in reducing the number of false positives, rather than enhancing detection accuracy. However, it is important to note that even with a fine vector mask, approximately 49.2% of the surface area of installed asbestos cement roofs remains undetected.

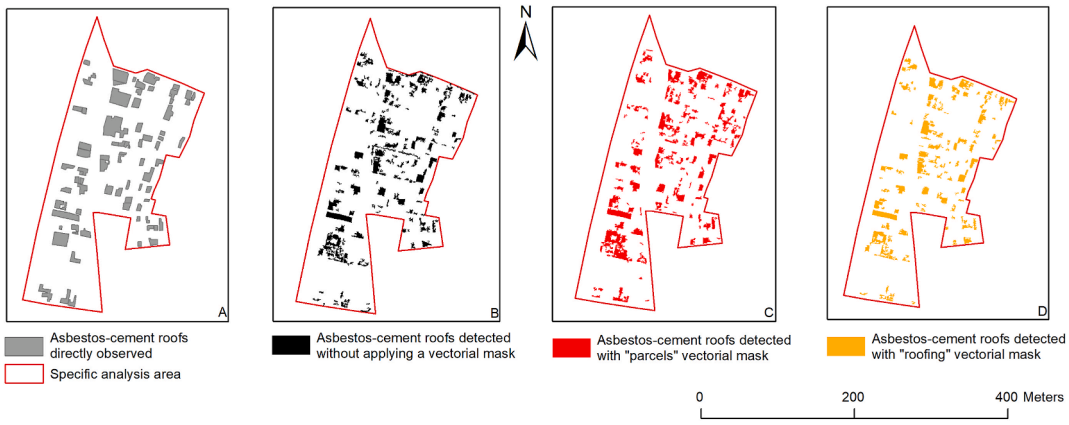

Fig. 5. Asbestos cement detected by RoofClassify in the Sibaté test area using different vector masks.

Table 4
Comparison of detection quality according to the vector mask used.

Vectorial mask	Areas of installed fiber-cement roofs (visual identification)	Areas of fiber-cement roofs detected by roofclassify	Concordance - Areas of fiber-cement roofs detected by roofclassify and validated by visual identification	False positive - Areas of fiber-cement roofs detected by roofclassify but not validated by visual identification	False negative - Areas of installed fiber-cement roofs not detected by roofclassify
without	6386,91m^2	5109,01m^2	3330.68m^2 (52.15%)	1775.11m^2 (34.74%)	3056.26m^2 (47.85%)
parcels	6386,91m^2	5382,77m^2	3406.52m^2 (53.34%)	1986.24m^2 (36.9%)	2980.53m^3 (46.66%)
roofing	6386,91m^4	4391,63m^2	3244.65m^2 (50.8%)	1144.2m^2 (26.05%)	3142.29m^2 (49.2%)

These results suggest that while a fine vector mask can help mitigate false-positive detections, it does not significantly improve the overall detection performance in terms of capturing all installed asbestos-cement surfaces. Therefore, other factors, such as the limitations of the classification algorithm or the resolution of the satellite imagery, may be contributing to the remaining undetected areas.

3.3. Overall performance analysis of the classification using a confusion matrix

An analysis of RoofClassify's performance through a pixel-oriented evaluation was conducted. The establishment of a general confusion matrix cross-referencing polygons related to the identification of four types of roofs with the classification produced by RoofClassify, based on the pansharpened image and cropped by the "parcels" vector mask, indicates an overall accuracy of 69.73% with a Kappa of 0.59, which can be considered moderate (Table 5). The classification performance of RoofClassify in our context varies depending on the type of roof: it is moderate for concrete identification (Kappa of 0.44) and satisfactory for identifying asbestos-cement (Kappa of 0.75).

3.4. Results of analyses of samples taken in critical areas

An additional validation step was conducted, involving the collection of samples for laboratory confirmation from unusual or unexpected locations where the plugin indicated the presence of asbestos-cement material. This verification process took place at a bullring and on an athletic track surrounding a football field. The bullring stands are constructed from concrete, and accordingly, a sample was collected from the stands.

Additionally, numerous patches on the surface of the athletic track were flagged as asbestos-cement. Six locations on the athletic track were sampled, with each location yielding samples from both the surface and 4 cm below the surface. These samples underwent analysis using PCM, SEM, and TEM at the University of Turin laboratories.

Of note, only one sample from a specific location on the athletic track, collected 4 cm below the surface, reported the presence of tremolite asbestos. This type of asbestos is typically associated with contamination rather than intentional use. This finding confirmed that the initial reports of asbestos-cement at the bullring and the athletic track were false positives.

4. Discussion

4.1. Strengths of the study

The classification performed by RoofClassify demonstrates a significant capability to accurately detect 53% of the installed asbestos-cement roofs area in Sibaté. When considering the overall accuracy of the classification tool across all types of roofs at the pixel level, the study achieves a value of 69.73%. Although this is lower than the 81.77% accuracy achieved in the Italian study (Tommasini et al., 2019), it still represents a meaningful detection rate.

Nevertheless, it is very important to note that, in this study, asbestos-cement was identified by RoofClassify—at least partially—in nearly 95% of the roofs where the presence of this material was confirmed in the test area (i.e., 78 visually confirmed asbestos-cement

Table 5
Precision matrix (asbestos-cement 1, concrete 2, clay tiles 3, zinc 4).

V_Classified	> ERROR MATRIX (pixel count)				
	1	2	3	4	Total
1	37080	6140	870	188	44278
2	7661	9711	321	501	18194
3	12564	2333	32400	5156	52453
4	6921	6498	1199	58503	73121
Total	64226	24682	34790	64348	188046
V_Classified	> AREA BASED ERROR MATRIX				
	1	2	3	4	Area
1	0.1672	0.0277	0.0039	0.0008	126236.7900
2	0.0733	0.0929	0.0031	0.0048	110066.2200
3	0.0839	0.0156	0.2163	0.0344	221473.3500
4	0.0261	0.0245	0.0045	0.2209	174623.3100
Total	0.3505	0.1607	0.2278	0.2610	632399.6700
Area	221639	101622	144089	165051	632399
SE	0.0010	0.0008	0.0008	0.0006	
SE area	646	531	496	411	
95% CI area	1266	1041	972	806	
PA [%]	47.6971	57.8101	94.9436	84.6489	
UA [%]	83.7436	53.3747	61.7696	80.0085	
Kappa hat	0.7497	0.4445	0.5049	0.7295	

Global accuracy [%]69.7311.
Kappa hat classification = 0.5965.

roofs). This indicates the generation of false negatives by RoofClassify, which can be explained by the proximity of spectral signals between visually similar roofs. Conversely, it demonstrates the significant capability of this plugin to identify asbestos-cement. This makes the tool potentially valuable for identifying asbestos-affected areas, enhancing territorial knowledge, and supporting asbestos removal strategies. The double sieving classification cleaning process helps reduce the number of pixels associated with false-positive noise, improving the overall accuracy of the results. Furthermore, using a "parcels" vector mask provides a balance between computational efficiency and maintaining satisfactory accuracy in identifying asbestos-cement roofs. This choice offers faster processing speeds while preserving reasonably good quality in classification outcomes.

4.2. Weaknesses and limitations

However, the study has several limitations that need to be addressed. The technique is prone to generating false-positive surfaces on materials or structures with similar colors to asbestos-cement, such as aged concrete or asphalt. For instance, the Plaza de Toros (Bull ring), which appears to be degraded concrete and the athletics track, composed of small greyish rock fragments, were mistakenly classified as asbestos-cement roofs. As mentioned earlier, the classification method relies on the signals acquired by the spectral bands of the WorldView-3, in the visible and near-infrared regions. Unfortunately, these spectral bands are not narrow enough to perform a fine spectral analysis of the sensed targets, which is the primary cause of detection errors. Additionally, the classification tool tends to classify all bare or partially bare soil as "tile" (representing clay roofing), making RoofClassify highly sensitive to soil characteristics. This bias is exacerbated when using a "parcels" vector mask, as it automatically classifies non-built elements as tiles.

To gain a better understanding of this bias, a simple comparison between the classification without a vector mask and the classification with a "roofing" vector mask is helpful (Fig. 6). These observations highlight the need for careful interpretation and validation of the classification results, considering the specific characteristics and limitations of the classification tool. Finally, the choice of vector mask may depend on the specific context and characteristics of the study area. Local conditions, data quality, and analysis objectives should all be considered when selecting the most appropriate vector mask for asbestos-cement detection.

Despite these limitations, combining RoofClassify's capabilities with subsequent on-site assessments can enhance the accuracy and reliability of asbestos detection efforts. Through this study, RoofClassify demonstrates encouraging performance in two very different urban contexts in Italy and Colombia. Scaling up is feasible and primarily constrained by the spatial extent of the satellite images used. The main limitation would then be the time required to analyze larger areas. The uniqueness of Sibaté also lay in its topography, which facilitated the visual identification of both training layers and control roofs. For future work, using a drone equipped with a high-resolution camera could be a moderately costly solution to replicate this approach in other regions.

5. Conclusion

One of the main advantages of the procedures and tools presented in this study, are the potential applicability in low- and middle-income countries because of their low cost (*i.e.*, the satellite images have a reasonable price if the area studied is not too vast, and the RoofClassify plugin is open access), the accuracy of detection of asbestos-cement roofing is not strongly dependent on the precision of

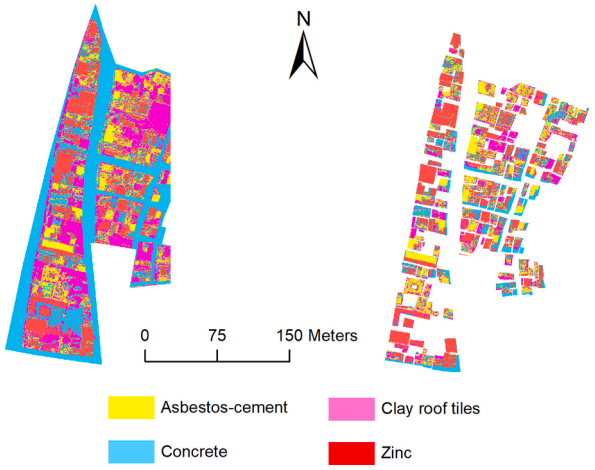

Fig. 6. Comparison of classifications without vector mask (left) and "roof" vector mask (right) on the test area.

input data (*i.e.*, vector masking), and because of the latter, it is potentially adaptable to the limitation in the quality of geospatial data frequently found in these type of countries.

On the other hand, the application of RoofClassify in Sibaté resulted in large false positive and false negative detection rates for asbestos roofing. Thus, in future applications of the plugin we suggest increasing the number of training layers and the number of polygons within each training layer, to explore if the accuracy improves.

Despite the limitations found and the structure of local roofs typically made up of an assembly of several types of materials over small areas, the plugin detects the partial presence of asbestos-cement roofs in 95% of the polygons that correspond to roofs in which this material has been visually confirmed.

Although asbestos-cement products release asbestos fibers over time due to deterioration of the encapsulating material, friable asbestos materials pose a much higher health risk (Lee and Kim, 2021b) (Government of Western Australia and Department of Health). Therefore, the decision to remove corrugated asbestos-cement sheets should be based on a technical assessment of the material's condition, as the replacement process can lead to asbestos exposure (Government of Western Australia and Department of Health) (UK Health Security Agency, 2024). Consequently, the management of corrugated asbestos-cement sheets should be guided by rigorous risk management plans (Government of Western Australia and Department of Health) (UK Health Security Agency, 2024).

In summary, the study introduces a novel application by integrating our methodology in a unique context. We have clarified the differences between the geographical areas of the first study and Sibaté, demonstrating how the change in context has modified the quality of the information used, such as cadastral data. Despite the limitations and varying quality of the information, RoofClassify shows encouraging results, highlighting its adaptability and reliability even with suboptimal data quality. Furthermore, our analysis of the changes implemented shows how they have affected the accuracy of our results in the Colombian context. This demonstrates its potential applicability across different regions worldwide. Additionally, RoofClassify is notable not only for its effectiveness but also for its affordability and accessibility. It is freely available and user-friendly, requiring no expert knowledge to be used effectively, which makes it a practical tool for a wide range of users.

Funding sources

This study has been funded with a grant from the French ANR (program ERASEd - ANR-18-CE03-0001-01). Francesco Turci acknowledge support from the Project CH4.0 under the MUR program "Dipartimenti di Eccellenza 2023–2027" (CUP: D13C22003520001)

Ethics

N/A.

Ethical statement

I, Benjamin Lysaniuk, hereby affirm that the manuscript titled "*Remote Detection of Asbestos-Cement Roofs: Evaluating a QGIS Plugin in a low- and middle-income country*" meets the following criteria.

1 - The content presented is entirely original and has not been published previously.
2 - The manuscript is exclusive to this submission and is not under consideration for publication elsewhere.
3 - The research and analysis presented in the paper are genuine and complete, reflecting the authors' own efforts.
4 - Proper acknowledgment is given to all co-authors for their significant contributions.
5 - The findings are appropriately situated within the context of prior and existing research.

6 - All sources referenced in the manuscript are accurately cited.
7 - Each author has actively participated in substantial work leading to the paper and accepts public accountability for its contents.

CRediT authorship contribution statement

Pauline Gluski: Writing – review & editing, Investigation, Formal analysis, Data curation. **Juan Pablo Ramos-Bonilla:** Writing – review & editing, Methodology, Investigation, Funding acquisition, Data curation. **Jasmine R. Petriglieri:** Writing – review & editing, Investigation. **Francesco Turci:** Writing – review & editing, Investigation. **Margarita Giraldo:** Writing – review & editing, Investigation. **Maurizio Tommasini:** Writing – review & editing. **Gabriele Poli:** Writing – review & editing. **Benjamin Lysaniuk:** Writing – original draft, Project administration, Methodology, Investigation, Funding acquisition, Formal analysis, Data curation, Conceptualization.

Declaration of competing interest

The authors declare the following financial interests/personal relationships which may be considered as potential competing interests:

Benjamin LYSANIUK reports financial support was provided by French National Research Agency. Francesco Turci reports financial support was provided by Ministry of University and Research. Juan Pablo Ramos-Bonilla provided, ad honorem, expert opinion in the Colombian Senate in the discussion of a Law banning asbestos in the country. If there are other authors, they declare that they have no known competing financial interests or personal relationships that could have appeared to influence the work reported in this paper.

Acknowledgements

We would like to warmly thank the Oslandia experts - Quy Thy Truong and Julien Moura - for the update service of the RoofClassify plugin as well as the Italian developers who authorized this update.

Data availability

Data will be made available on request.

References

Abbasi, M., Mostafa, S., Vieira, A.S., Patorniti, N., Stewart, R.A., 2022. Mapping roofing with asbestos-containing material by using remote sensing imagery and machine learning-based image classification: a state-of-the-art review. Sustainability 14 (13), 8068. https://doi.org/10.3390/su14138068.
Ascolfibras, CONCEPTO DE ASCOLFIBRAS DEL PROYECTO DE LEY NÚMERO 97 DE 2015 SENADO, Bogotá, mayo 4 de 2016.
Borfecchia, F., et al., 2010. Active and passive remote sensing for supporting the evaluation of the urban seismic vulnerability. Italian Journal of Remote Sensing 42 (3), 129–141.
Btown, S., 2021. Machine Learning, Explained. MIT Management Sloan School. URL: https://mitsloan.mit.edu/ideas-made-to-matter/machine-learning-explained. Accessed on June 2023.
Campopiano, A., Ramires, D., Zakrzewska, A.M., Ferri, R., D'annibale, A., Pizzutelli, G., 2009. Risk assessment of the decay of asbestos cement roofs. Ann. Occup. Hyg. 53 (6), 627–638. https://doi.org/10.1093/annhyg/mep036.
Cely-García, M.F., Lysaniuk, B., Pasetto, R., Ramos-Bonilla, J.P., 2020. The challenges of applying an Activity-Based Sampling methodology to estimate the cancer risk associated with asbestos contaminated landfilled zones. Environ. Res. 181, 1–10. https://doi.org/10.1016/j.envres.2019.108893.
Congedo, L., 2021. Semi-Automatic Classification Plugin: a Python tool for the download and processing of remote sensing images in QGIS. J. Open Source Softw. 6 (64), 3172. https://doi.org/10.21105/joss.03172.
Congreso de Colombia, 2019. Ley 1968 de 2019. Por la cual se prohíbe el uso de asbesto en el territorio nacional y se establecen garantías de protección a la salud de los colombianos. Available at: https://dapre.presidencia.gov.co/normativa/normativa/LEY/201968/20DEL/2011/20DE/20JULIO/20DE/202019.pdf. Accessed June 2023.
Dyczek, J., 2006. Surface of asbestos-cement (AC) roof sheets and assessment of the risk of asbestos release. Paper Presented at International Seminar on Asbestos Risk Reduction & Measurement of Asbestos Fibre Concentration. Cracow, Poland.
Ervik, T., Hammer, S.E., Graff, P., 2021. Mobilization of asbestos fibers by weathering of a corrugated asbestos cement roof. J. Occup. Environ. Hyg. 18 (3), 110–117. https://doi.org/10.1080/15459624.2020.1867730.
Fiumi, L., Campopiano, A., Casciardi, S., et al., 2012. Method validation for the identification of asbestos-cement roofing. Appl Geomat 4, 55–64. https://doi.org/10.1007/s12518-012-0078-0.
Flórez Gutiérrez, P., Cely-García, M.F., Larrahondo, J.M., 2023. Environmental management criteria, aimed at public policymaking, for the removal and disposal of asbestos-containing building materials in Colombia. Integrated Environ. Assess. Manag. 19, 1079–1088. https://doi.org/10.1002/ieam.4736.
Frassy, F., Candiani, G., Rusmini, M., Maianti, P., Marchesi, A., Nodari, F.R., Via, G.D., Albonico, C., Gianinetto, M., 2014. Mapping asbestos-cement roofing with hyperspectral remote sensing over a large mountain region of the Italian western alps. Sensors 14 (9), 15900–15913. https://doi.org/10.3390/s140915900.
Gassar, A.A.A., Cha, S.H., 2021. Review of geographic information systems-based rooftop solar photovoltaic potential estimation approaches at urban scales. Appl. Energy 291, 116817. https://doi.org/10.1016/j.apenergy.2021.116817.
Gibril, M.B.A., Shafri, H.Z.M., Hamedianfar, A., 2017. New semi-automated mapping of asbestos cement roofs using rule-based object-based image analysis and Taguchi optimization technique from WorldView-2 images. Int. J. Rem. Sens. 38 (2), 467–491. https://doi.org/10.1080/01431161.2016.1266109.
Government of Western Australia, Department of Health, Guidance Note on Asbestos Cement Roofs. Available at: https://www.health.wa.gov.au/-/media/Files/Corporate/general-documents/Asbestos/PDF/GuidanceNoteonAsbestosCementRoofs20162-1.pdf.
Health and Safety Executive, 2021. Asbestos: the analysts' guide for sampling, analysis and clearance procedures, Executive Health and Safety, second ed. HSE Books, p. 238. HSG248.
Hikuwai, M.V., Patorniti, N., Vieira, A.S., Frangioudakis, Khatib G., Stewart, R.A., 2023. Artificial intelligence for the detection of asbestos cement roofing: an investigation of multi-spectral satellite imagery and high-resolution aerial imagery. Sustainability 15 (5), 4276. https://doi.org/10.3390/su15054276.
IARC, 2012. IARC Monographs on the Evaluation of Carcinogenic Risks to Humans. Asbestos (Chrysotile, Amosite, Crocidolite, Tremolite, Actinolite, and Anthophyllite, 100C.
INSERM (collective expertise), 1997. Health Effects of the Main Types of Exposure to Asbestos, Les éditions Inserm, Paris, p. 434. Report.
Introduction to deep learning, ESRI. URL: https://pro.arcgis.com/en/pro-app/2.9/help/analysis/deep-learning/what-is-deep-learning-.htm (Accessed on June 2023).

Jakhar, D., Kaur, I., 2020. Artificial intelligence, machine learning and deep learning: definitions and differences. Clin. Exp. Dermatol. 45 (1), 131–132. https://doi.org/10.1111/ced.14029.
Kaplan, G., Gašparović, M., Kaplan, O., Adjiski, V., Comert, R., Mobariz, M.A., 2023. Machine learning-based classification of asbestos-containing roofs using airborne RGB and thermal imagery. Sustainability 15 (7), 6067. https://doi.org/10.3390/su15076067.
Kononenko, I., 2001. Machine learning for medical diagnosis: history state of art and perspective. Artif. Intell. Med. 23 (1), 89–109. https://doi.org/10.1016/S0933-3657(01)00077-X.
Kottek, M., Yuen, M.L., 2022. Public health risks from asbestos cement roofing. Am. J. Ind. Med. 65, 157–161. https://doi.org/10.1002/ajim.23321.
Krówczyńska, M., Raczko, E., Staniszewska, N., Wilk, E., 2020. Asbestos-cement roofing identification using remote sensing and convolutional neural networks (CNNs). Rem. Sens. 12 (3), 408. https://doi.org/10.3390/rs12030408.
Lee, E.S., Kim, Y.K., 2021a. Asbestos exposure level and the carcinogenic risk due to corrugated asbestos-cement slate roofs in korea. Int. J. Environ. Res. Publ. Health 18 (13), 6925. https://doi.org/10.3390/ijerph18136925.
Lee, E.S., Kim, Y.K., 2021b. Asbestos exposure level and the carcinogenic risk due to corrugated asbestos-cement slate roofs in korea. Int. J. Environ. Res. Publ. Health 18 (13), 6925. https://doi.org/10.3390/ijerph18136925. PMID: 34203418; PMCID: PMC8297172.
Li, Z., Wang, Y., Zhang, N., Zhang, Y., Zhao, Z., Xu, D., Ben, G., Gao, Y., 2022. Deep learning-based object detection techniques for remote sensing images: a survey. Rem. Sens. 14, 2385. https://doi.org/10.3390/rs14102385.
Lysaniuk, B., Cely-García, M.F., Mazzeo, A., Marsil, D., Pasetto, R., Comba, P., Ramos-Bonilla, J.P., 2020. Where are the landfilled zones? Use of historical geographic information and local spatial knowledge to determine the location of underground asbestos contamination in Sibaté (Colombia). Environ. Res. 191, 110182. https://doi.org/10.1016/j.envres.2020.110182.
Maxwell, A.E., Warner, T.A., Fang, F., 2018. Implementation of machine-learning classification in remote sensing: an applied review. Int. J. Rem. Sens. 39 (9), 2784–2817. https://doi.org/10.1080/01431161.2018.1433343.
Mohajeri, N., et al., 2018. A city-scale roof shape classification using machine learning for solar energy applications. Renew. Energy 121, 81–93. https://doi.org/10.1016/j.renene.2017.12.096.
Osińska-Skotak, K., Ostrowski, W., 2015. Use of satellite and ALS data for classification of roofing materials on the example of asbestos roof tile identification. Technical Sciences 18 (4), 283–298.
Ozbayoglu, A.M., Gudelek, M.U., Sezer, O.B., 2020. Deep learning for financial applications: a survey. Appl. Soft Comput. 93, 106384. https://doi.org/10.1016/j.asoc.2020.106384.
Parki, Woolf B., 2009. Chapter 7 - machine learning. In: Building Intelligent Interactive Tutors Student-Centered Strategies for Revolutionizing E-Learning. pp. 221–297. https://doi.org/10.1016/B978-0-12-373594-2.00007-1.
Petriglieri, J., Laporte-Magoni, C., Gunkel-Grillon, P., Tribaudino, M., Bersani, D., Sala, O., Mestre, M., Vigliaturo, R., Bursi, Gandolfi N., Salvioli-Mariani, E., 2020. Mineral fibres and environmental monitoring: a comparison of different analytical strategies in New Caledonia. Geosci. Front. 11, 189–202. https://doi.org/10.1016/j.gsf.2018.11.006.
Ramos-Bonilla, J.P., Cely-García, M.F., Giraldo, M., Comba, P., Terracini, B., Pasetto, R., et al., 2019. An asbestos contaminated town in the vicinity of an asbestos-cement facility: the case study of Sibaté, Colombia. Environ. Res. 176, 108464. https://doi.org/10.1016/j.envres.2019.04.031.
Shebab, M., et al., 2022. Machine learning in medical applications: a review of state-of-the-art methods. Comput. Biol. Med. 145, 105459. https://doi.org/10.1016/j.compbiomed.2022.105458.
Spurny, K.R., 1989. Asbestos fibre release by corroded and weathered asbestos-cement products. IARC Sci. Publ. 90, 367–371. . PMID: 2744837.
Szabó, S., Burai, P., Kovács, Z., Szabó, G., Kerényi, A., Fazekas, I., Paládi, M., Buday, T., Szabó, G., 2014. Testing algorithms for the identification of asbestos roofing based on hyperspectral data. Environ. Eng. Manag. J. 143, 2875–2880. https://doi.org/10.30638/eemj.2014.323.
Taherzadeh, E., Shafri, H.Z.M., 2013. Development of a generic model for the detection of roof materials based on an object-based approach using WorldView-2 satellite imagery. Adv. Rem. Sens. 2 (4), 312–321. https://doi.org/10.4236/ars.2013.24034.
Tommasini, M., Bacciottini, A., Gherardelli, M., 2019. A QGIS tool for automatically identifying asbestos roofing. ISPRS Int. J. Geo-Inf. 8 (3), 131. https://doi.org/10.3390/ijgi8030131.
Trevisiol, F., Lambertini, A., Franci, F., Mandanici, E., 2022. An object-oriented approach to the classification of roofing materials using very high-resolution satellite stereo-pairs. Rem. Sens. 14 (4), 849. https://doi.org/10.3390/rs14040849.
UK Health Security Agency, 2024. Asbestos general information. available at: https://www.gov.uk/government/publications/asbestos-properties-incident-management-and-toxicology/asbestos-general-information.
Valdelamar, Martinez D.E., Saba, M., Torres Gil, L.K., 2024. Assessment of asbestos-cement roof distribution and prioritized intervention approaches through hyperspectral imaging. Heliyon 10 (3), e25612. https://doi.org/10.1016/j.heliyon.2024.e25612.
Virta, R.L., 2006. Worldwide Asbestos Supply and Consumption Trends from 1900 through 2003, 1298. U.S. Geological Survey Circular, p. 80. Available online at: https://pubs.usgs.gov/circ/2006/1298/c1298.pdf.
Walter, V., 2004. Object-based classification of remote sensing data for change detection. ISPRS J. Photogrammetry Remote Sens. 58 (3–4), 225–238. https://doi.org/10.1016/j.isprsjprs.2003.09.007.
Yuan, X., Shi, J., Gu, L., 2021. A review of deep learning methods for semantic segmentation of remote sensing imagery. Expert Syst. Appl. 169, 114417. https://doi.org/10.1016/j.eswa.2020.114417.